Title: Additive manufacture of multistable structures

Authors: Evripides G. Loukaides[1]*, Rhodri W.C. Lewis[2], Christopher R. Bowen[1]

Affiliations:

[1]Department of Mechanical Engineering, University of Bath, BA2 7AY, UK.

[2]Renishaw PLC, GL12 8JR, UK.

*Correspondence to: e.loukaides@bath.ac.uk

Abstract:

Residual thermal stresses which develop during additive manufacturing processes are often a cause of unwanted component deformation and mechanical failure. We demonstrate that this impairment can in fact be exploited to enhance the design process for shell structures, where bistability is known to emerge in particular instances due to the presence of inelastic stresses. Multistable structures are produced through a single additive manufacturing operation by considering the inherent availability of thermal stresses in certain additive technologies. This concept is demonstrated through an analytical example, numerical simulations and a physical demonstrator produced via Selective Laser Sintering of a titanium alloy. Our findings underline these hitherto untapped capabilities of additive processes and facilitate a deeper understanding of the thermal stresses developed during manufacture.

Introduction

The availability of multistable geometries in shell structures with certain mechanical properties or prestressing is now well understood [1]. However, the manufacture of these structures has not yet matured, preventing their widespread application. To date, the prevalent means of constructing multistable shells have been multi-step and multi-material methods, such as the curing of composite laminates or the manufacture of corrugated metallic shells. In this work, we exploit a known ingredient of multistability (prestressing), and a topical additive manufacturing method (Selective Laser Sintering or SLS), to produce a bistable shell in a single operation and a single material.

In recent decades, the multistability of thin structures with tailored material properties and geometry has been studied extensively. The popularity of the topic can be tied to the emergence of composite laminates as suitable materials for this category of structures [2]. Laminates have been an attractive material for the creation of multistable shells since they allow bespoke mechanical properties by control of the laminate layup and can withstand significant loads; in this case, bistability arises from the anisotropic thermal expansion of the individual laminate layers. The literature provides a plethora of examples examining both the necessary laminate layup and the influence of the curing process on the resulting stable geometries [3,4]. Prestressing of fibres has also been employed to induce bistability [5,6]. However, composite laminates present several obstacles, including limited scalability in terms of manufacture of small-scale composites and significant processing costs.

An overview of smart structures and potential applications that employ bistability and buckling can be found in [7]. Applications in constructing non-linear energy harvesters have been popular and present improved efficiency compared to their linear counterparts [8,9]. By combining bistable elements, variable stiffness structures can be constructed, opening up opportunities for morphing skins in aerospace applications [10] and vibration isolation [11]. Metallic bistable structures have included the uses of bimetallic strips where their thermo-mechanical properties have been exploited to construct micro-electro-mechanical system

(MEMS) based heat engines [12,13]. At the microscale, metallic bistable membranes have also been considered as components for switches, micro-valves and micro-pumps [14]. These systems are notably complex to manufacture but suggest a range of new applications at this small scale, including mechanical memory devices [15].

Bistability also emerges in metallic sheets due to plastic strains [16]. In addition, material patterning has been used to induce multistability, and to provide alternative material and manufacturing options. Some examples include dimples [17] and corrugations [18], though, the manufacturing methods involve plastic deformation and are therefore likely to result in built-in stresses within the structure. More recently, a cylindrical square honeycomb, made from a homogeneous material without prestressing, was shown to be bistable [19]. We can see that common factors of existing methods to create bistable laminate and metallic shells are complexity, and limited scope in terms of geometry and scale.

Selective Laser Sintering (SLS) is gaining traction as a highly capable process, particularly for the manufacture of structurally optimal structures in the aerospace industry. In this process, a powder bed is heated locally, binding the melted powder, and thus creating 3D structures, layer by layer. Along with stereo-lithography (SLA) and Fused Deposition Modelling (FDM), these processes are often referred to as '3D printing'. Originally, 3D printing was mostly employed for prototyping, but continuous improvements to the process have signaled a promising future for industry-grade applications. Part of the appeal of these technologies is the immediate access to complex geometries, with limited waste of material and without the need for dedicated tools. In addition, no expert labor is required, as is the case for composite laminates and as the technology improves, they can operate at a range of scales. Finally, the decreasing cost of 3D printers allows access to a wide range of makers, including home users.

The newly available characteristics of 3D-printed materials have inspired some recent work, which focuses on morphing capabilities. In [20], a Smart Soft Composite (SSC) 3D-printed material with morphing capabilities is introduced. This material, however, relies on similar mechanics to laminates. Other 3D-printed designs seek to produce bistability by relying on boundary conditions and "architectured materials" [21,22] – in contrast, this work relies on an intrinsic form of bistability which is simple to implement and provides greater design freedom. Recently, residual stresses in the Direct Laser Writing process were employed to induce programmable, self-bending behavior [23]. More generally, the emerging interest in 3D printing and morphing structures culminates in a category of structures termed "4D materials" – materials with a prescribed behaviour over time. A review with examples at various scales is given in [24].

The theoretical treatment of multistable shells frequently employs the Föppl-Von Kármán equations and assumes that the shell is characterized by spatially uniform curvatures. This originated in work by Mansfield [25], but subsequently a number of contributors refined the model [26–28] to allow investigation of more complex behavior and actuation strategies to induce snap-through between stable states. Recent results include the possibility of constructing tristable shells [29] and the availability of engineered neutrally stable/zero stiffness shells [30], which facilitate exciting new applications, such as gear-less motors [31]. As these technologies approach maturity, higher degree of freedom (DOF) models are needed to examine intermediate geometries [32,33] and the effects of boundary constraints [34,35].

We present a new route towards designing and manufacturing a bistable shell using a single material and exploiting the residual thermal stresses inherently present in SLS.For an analytical approach to this design, previous work by Seffen and Guest [30] is employed. The uniform curvature (UC) model constructs the strain energy of a free-standing shell at any

configuration as a sum of bending and stretching contributions if its curvatures remain spatially uniform. This formulation incorporates parameters that describe material properties, the initial geometry and – aptly for this application – inelastic curvatures in the shell. These inelastic curvatures can be used to describe a variety of imposed strains including those encountered in growth and plastic deformation. Here, they are used to capture the thermo-mechanical stresses induced in the shell by differential cooling of the metal during SLS.

Analytical background

Following the energy formulation for elliptical shells found in [36,37], the resulting dimensionless strain energy expression, U, can produce solutions for equilibrium geometries by setting its partial derivatives with respect to the three observed curvatures (κ_x, κ_y, κ_{xy},) to zero:

$$\kappa_x + \mu\,\kappa_y \;=\; \kappa_{x0} + \nu\,\kappa_{y0} \;+ \kappa_{xp} \;+ \nu\,\kappa_{yp} \tag{1}$$

$$\mu\,\kappa_x + \kappa_y = \nu\,\kappa_{x0} + \;\kappa_{y0} \;+ \nu\,\kappa_{xp} \;+ \kappa_{yp} \tag{2}$$

$$(2\alpha + \nu - \mu)\kappa_{xy} \;=\; 2\,\alpha\,\kappa_{xy0} \tag{3}$$

where

$$\mu \;\; = \nu + \phi\,\Delta g \;= \nu + \phi\big(\kappa_{\mathrm{x}}\,\kappa_{\mathrm{y}} \;- \kappa_{\mathrm{xy}}^2 \;- \kappa_{\mathrm{x0}}\,\kappa_{\mathrm{y0}} \;+ \kappa_{\mathrm{xy0}}^2\big) \tag{4}$$

All the curvatures are given in a dimensionless form, with the subscripts 0 and p indicating initial and prestress respectively and x, y indicating orthogonal directions on the tangent plane of the shell – the directions are indicated in Fig. 2, Fig. 4 and Fig. 6 for a relevant demonstrator, which is described in a subsequent section. The parameter ν is the Poisson ratio and α is equal to $(1-\nu)/2$ for an isotropic material. The factor ϕ combines various geometric and material parameters:

$$\phi = (b^4)/(t^2\,R^2) \times\; (1-\nu^2)\alpha/(3\alpha + (1-\nu^2-2\nu\alpha)\rho^2 \;+\; 3\alpha\,\rho^4) \tag{5}$$

For the isotropic case, we substitute α to get:

$$\phi = \;\{b^4\,(1-\nu^2)\}/[(3\,\rho^4 \;+ 2\,\rho^2 + 3)R^2\,t^2] \tag{6}$$

where t is the shell thickness; $2a$, $2b$ are the major and minor axes and $\rho = b/a$; R is the characteristic radius of curvature of the shell, which allows the dimensionless form to emerge. Although this model was initially developed for elliptical shells, Hamouche *et al* (*1*) demonstrated that a correction by a factor allows the expression to be applicable to rectangular shells.

The stability of resulting solutions can be examined by considering the Hessian of the dimensionless strain energy, H.

$$H = \begin{bmatrix} 1+\phi\kappa_y^2 & \mu+\phi\,\kappa_x\,\kappa_y & -2\phi\,\kappa_y\kappa_{xy} \\ \mu\;+\phi\,\kappa_x\,\kappa_y & 1\;+\phi\,\kappa_x^2 & -2\phi\,\kappa_x\,\kappa_{xy} \\ -2\phi\,\kappa_{xy}\,\kappa_y & -2\phi\,\kappa_{xy}\kappa_x & \alpha\;-\;2\phi\,\Delta g\;+\;4\phi\,\kappa_{xy}^2 \end{bmatrix} \tag{7}$$

Solutions with a positive-definite H are judged as stable. Following this, the problem of an initially cylindrical, isotropic shell with same-sense prestressing can be reduced to the following system of equations, with the curvatures of the shell as an unknown:

$$\kappa_x + \mu\,\kappa_y \;=\; \kappa_0 + (1+\nu)\,\kappa_p \tag{8}$$

$$\mu\,\kappa_x + \kappa_y = \nu\,\kappa_0 + \;(1\;+\nu)\kappa_p \tag{9}$$

$$(1-\mu)\kappa_{xy} = 0 \tag{10}$$

$$\mu = \nu + \phi\left(\kappa_x \kappa_y - \kappa_{xy}^2\right) \tag{11}$$

From Eqs. 8-10, for an initial curvature to be present, twisted solutions are not available, since this would require $\kappa_0 = \nu\kappa_0$. Hence, we can also ignore Eq. 8, and assume $\kappa_{xy} = 0$. For arbitrary κ_0 and κ_p there is no tractable solution, but some analytical solutions by considering a sub-case. We consider a combination of initial curvature and prestressing that produces opposite quantities on the right-hand side of Eqs 8 and 9. This can be achieved by setting $\kappa_0 = -2\kappa_p$, such that the system becomes:

$$\kappa_x + \mu\,\kappa_y = -(1-\nu)\,\kappa_p \tag{12}$$

$$\mu\,\kappa_x + \kappa_y = (1-\nu)\kappa_p \tag{13}$$

If we only admit untwisted solutions, such that $\kappa_{xy} = 0$, then Eq. 10 is satisfied. This can be done without loss of generality by considering x and y as principal directions. One solution to this system, by symmetry, is $\kappa_x = -\kappa_y = \kappa$, i.e. a saddle shape. Combined with Eq. 11 in the form, $\mu = \nu - \phi\kappa^2$, the system reduces to:

$$\kappa + \frac{\phi\kappa^3}{1-\nu} = \kappa_p$$

The solution to this represents monostable behavior, with κ increasing monotonically with κ_p as per (*26*). By inspection, the system is additionally satisfied when $\mu = -1$. After substituting this value, Eqs 12 and 13 reduce to:

$$\kappa_x - \kappa_y = -(1-\nu)\kappa_p \tag{14}$$

while for untwisted solutions, Eq. 11 becomes:

$$\kappa_x\,\kappa_y = -\frac{1+\nu}{\phi} \tag{15}$$

The resulting quadratic equation can be solved for either κ_x or κ_y, and then with substitution, we produce the principal curvatures as:

$$\kappa_x = -\frac{(1-\nu)}{2}\kappa_p\left(1 \pm \sqrt{1 - \frac{\left(4(1+\nu)\right)}{\left(\kappa_p^2\,\phi(1-\nu)^2\right)}}\right) \tag{16}$$

$$\kappa_y = \frac{(1-\nu)}{2}\kappa_p\left(1 \pm \sqrt{1 - \frac{\left(4(1+\nu)\right)}{\left(\kappa_p^2\,\phi(1-\nu)^2\right)}}\right) \tag{17}$$

These represent two possible geometries, available past a bifurcation point, such that:

$$\frac{4(1+\nu)}{\kappa_p^2\phi(1-\nu)^2} < 1 \tag{18}$$

or

$$|\kappa_p| > \sqrt{\frac{4(1+\nu)}{\phi(1-\nu)^2}} \tag{19}$$

which gives the critical value for bistability to emerge for this ratio of initial curvature and pre-stress. For large values of prestressing, κ_p, the stable geometries asymptotically approach cylindrical shapes, see Fig. 1A. More generally, the system can be approached numerically, by obtaining equilibrium solutions and then testing their stability. A colourmap of the monostable and bistability regions for different combinations of initial curvature, κ_0, and prestress, κ_p, can be generated, as shown in Fig. 1D. The graphical overview provided there, establishes the availability of bistability beyond the specific case investigated above. Indeed, the development of residual stresses in SLS is not yet fully understood, and prescribing their magnitude is not a trivial task.

Physical and numerical verification

A demonstrator was constructed by sintering Ti-6Al-4V powder to establish the potential of prestressing curved shell structures through SLS to create multistable structures. A spiral pattern was constructed with a single pass per layer, using a Renishaw AM250 machine. The laser parameters for the spirals were 200W at 50μs exposure time in an argon inert gas atmosphere. The point distance was 60μm. The gap between each revolution was 0.6mm and the vector distance between points was 75μm. Additional cylindrical structures were printed separately. Specifically, six cylinders of radii 5, 6, 7, 8, 9 and 10mm where printed with a 1mm gap at the periphery. Both the cylindrical and spiral designs are shown in Fig. 2.

The as-built structures are shown in Fig. 2B, while still attached on the build plate. After removal from the build plate, substantial springback was observed – this is shown for cylindrical parts in Fig. 3A and is investigated later in this section. The spiral was then separated into three sections. The inner part is monostable, see Fig. 1B. At the same time, for intermediate sections of the spiral, a secondary stable geometry is available, as demonstrated by the single sample whose stable states are shown in Fig. 1E and Fig. 1F. These were scanned with a Proscan 2000 non-contact profilometer and digital representations were then used to calculate the initial dimensions of the structure as well as the curvature for both configurations. The thickness of the shell was similarly measured using a Leica M205C optical microscope. SLS parts are characterized by a non-smooth surface finish, seen in Fig. 4C, hence an average thickness was calculated at 87μm. The curvature of the shell initially was 15.1mm. In the second configuration, the curvature along the orthogonal direction to the initial curvature was 10.7mm. Inspection of the structure with magnification offers additional insights. In Fig. 5A and Fig. 5B the high degree of density can be observed to agree with the process set-up for Ti6Al4V on a Renishaw AM250 system (typical density ≥99.8% [38]). Scanning Electron Microscopy (SEM) images reveal the influence of the laser trajectory on the material flow and a distortion associated with the change in shape for the second geometry (Fig. 5C and Fig. 5D). No surface finishing was carried out which may be seen in the form of un-sintered powder.

The surface residual stresses for the bistable sample were measured along the axial and hoop directions of the cylindrical sample using X-Ray Diffraction (XRD). In preliminary measurements, the residual stresses were measured at points across one side of the shell, using a Pulstec, μ-X360n system VEQTER Ltd (Purchase Order 22027747). The measurements were made across a regular grid, at 56 points, with results shown in Fig. 4. Subsequently, additional measurements were made at five points on both sides of the sample by the AMRC, University of Sheffield (Project reference AS3256), using a Proto XRD device. The points are indicated in Fig. 2C and results are shown in Table 1. The measurements indicate a remarkably uniform distribution of stresses across both surfaces and in both configurations, and at the same time show that the underlying thermo-mechanical cause is not characterized by through-thickness symmetry. In the initial geometry, the most

prominent residual stresses are positive and in the axial direction. In the second geometry, residual stresses are predominantly negative and in the new axial direction – the curvature is now along the previous axial direction.

External sections of the spiral behave like a tape string and adopt a new geometry, that is they become (approximately) cylindrical in the opposite sense. Such a section is shown in Fig. 1G, where it is displayed along with the original build plate. In addition to the significant change in geometry, we observe that a twisting curvature is also present. This is true for the entirety of the spiral part after Electrical Discharge Machining removal from the build plate. Most notably, the latter section demonstrates how the residual stresses can be used to produce structures at a scale far exceeding the dimensions of the build plate.

Finite Element Analysis (FEA) for testing of the bistable behaviour concept in SLS manufactured shells was carried out on the commercial software package Abaqus. The structure is based on the geometry of the bistable sample above, i.e. initially a cylindrical shell. The mesh was composed of S4R elements, where S4R is a general purpose 4-node shell element with reduced integration and a large-strain formulation which also allows for the imposition of a through-thickness thermal gradient. The latter is needed to emulate the presence of thermal stresses in the shell. The dimensions of the virtual sample match the dimensions of the physical bistable sample detailed in the previous section. The material is based on the isotropic properties of annealed titanium Ti-6Al-4V alloy (Grade 5), taken from [39]. The modulus of elasticity is set at 110 GPa, the Poisson ratio at 0.33 and the coefficient of thermal expansion at 9×10^{-6} K^{-1}. Initially, the temperature across the model is zero. The analysis begins with an Implicit Static Step that imposes a temperature gradient (0-5100K) across the thickness of the shell. This is directed such that it generates a curvature in the opposite direction to the initial cylindrical curvature. At the end of this Step, the structure reaches an equilibrium and an updated geometry is made available with imposed prestress.

The bistability of the shell is then examined in two separate Dynamic Implicit Steps with a duration of 1s each and quasi-static application. All degrees of freedom of the central node of the shell structure are fixed, whereas the rest of the structure is unconstrained. In the first Step of the analysis, displacement control is applied on the four corners nodes of the shell, actuating the structure towards a second stable state, as shown in Fig. 6B. Only one degree of freedom on these nodes is controlled, corresponding to the direction orthogonal to the initial directions of principal curvatures. The nodes are moved past the initial height of the shell. In the second step, the displacement control is removed, and the shell is allowed, load free, to return to an equilibrium state. If, after the second step, the structure returns to the original geometry, this is deemed a monostable configuration. Otherwise, if a second equilibrium state is observed, the configuration is bistable. The stability of the configurations can also be confirmed by the progression of the strain energy in the structure during and after actuation. Similar actuation strategies are used in the literature to demonstrate or examine bistability physically or in simulations [19,31].

SLS parts are characterized by a non-smooth surface finish, seen in Fig. 2C, hence an average thickness was used for the model. The results confirm the availability of the bistable state for a prescribed ratio of inelastic to initial curvature. The thermal stresses were imposed at the start of the simulation using a through-thickness linear temperature gradient. In Fig. 7A and Fig. 7B, the calculated stresses on the surface of the shell are shown after the thermal gradient is imposed and again after the shell is actuated to a second stable state. A similar pattern to the XRD results is observed, although the applied thermal gradient results in symmetric surface stresses. The edge effects shown in the FEA results are not captured with XRD, likely because no sample points were close enough to the edge. In Fig. 7C, the strain

energy for the entire structure is plotted through the three steps of the simulation (thermal load, actuation past second state and relaxation to second state). This reveals the self-equilibrium energy, which is produced by the thermal stresses, as well as the second strain energy minimum, which characterizes the second stable geometry.

In addition, the printed open cylindrical shells were used to examine the influence of geometry on the resulting springback, and the emergence of bistability for increasing radii of curvature. The designed geometry as printed on the plate is shown in Fig. 2A, while the resulting initial geometries after springback are shown in Fig. 3A. The measured springback indicates that the initial radius, and, in effect, the laser scanning trajectory, does not correlate with the magnitude of the residual stresses, see Table 2. Instead, the small variations in imposed curvature do not follow any discernible pattern despite the change in geometry. We also note that the position on the build plate does not offer any observable correlation with springback either. Hence, although the emergence of residual stresses is reliable, the exact mechanism for its generation is not clear. Bistability is available for all the cylinders except the one with the smallest radius of curvature, where the residual stress seems insufficient to overcome the initial geometry, see Fig. 3B.

Considering the XRD data and given the absence of any other sources of anisotropy in heat dissipation, the laser path might explain the through-thickness thermal stress. The laser beam does not deliver energy uniformly on the surface and meets the workpiece at an angle. Residual stresses in the literature are typically studied for thick components and not for single-layer, thick components, hence this exact phenomenon is not noted. Recent work has indicated that locally asymmetric stresses can be explained by differential cooling initiated by non-uniform powder particles size [40], but this does not explain the persistence of the asymmetry at greater scales. We hypothesize that heat is introduced more readily on one side of the shell due to the curved path of the laser, which, in this instance, matches the design curvature of the shell; hence, a corresponding through-thickness stress is developed during cooling. Additional parameters, such as the orientation of the laser beam with respect to the location of each part on the build plate, might also influence the exact magnitude of stresses.

Concluding remarks

We have presented a new concept of additive manufacture that introduces the usefulness of intentionally incorporating residual stresses in the design of printed structures, using bistable shells as an example and demonstrator. A proven analytical model was used to demonstrate the necessary conditions with respect to geometry and residual stress for this behavior to be feasible, and the behaviour was confirmed both in FE simulations and via a physical demonstrator. An intentional use of residual stresses would enhance the ever-expanding applications for additive manufacturing technologies and would offer the designer an additional tool. Using this technique, a whole array of applications for multistable shells becomes more readily available thereby reducing relevant costs and assisting scalability. We note that integration of multistable behavior in sections of larger structures is straightforward, see Fig. 3C and Fig. 3D. This can include components at a range of geometries and scale, along with internal bistable elements for application such as valves, vibration suppression, non-linear stiffness, and structures that deploy with minimal activation energy. This approach also enables the construction of SLS printed parts that are no longer restricted to the size of the build plate.

References:

[1] Hamouche W, Maurini C, Vincenti A and Vidoli S 2016 Basic criteria to design and produce multistable shells *Meccanica* **51** 2305–20

[2] Hyer M W 1981 Calculations of the room-temperature shapes of unsymmetric laminates *J. Compos. Mater.* **15** 296–310

[3] Dano M-L and Hyer M W 1998 Thermally-induced deformation behavior of unsymmetric laminates *Int. J. Solids Struct.* **35** 2101–2120

[4] Giddings P F, Bowen C R, Salo A I T, Kim H a. and Ive A 2010 Bistable composite laminates: Effects of laminate composition on cured shape and response to thermal load *Compos. Struct.* **92** 2220–5

[5] Chillara V S C and Dapino M J 2017 Mechanically-prestressed bistable composite laminates with weakly coupled equilibrium shapes *Compos. Part B Eng.*

[6] Daynes S, Potter K D and Weaver P M 2008 Bistable prestressed buckled laminates *Compos. Sci. Technol.*

[7] Hu N and Burgueño R 2015 Buckling-induced smart applications: recent advances and trends *Smart Mater. Struct.* **24** 063001

[8] Arrieta A, Hagedorn P, Erturk A and Inman D 2010 A piezoelectric bistable plate for nonlinear broadband energy harvesting *Appl. Phys. Lett.* **97** 104102–104102

[9] Harne R and Wang K 2013 A review of the recent research on vibration energy harvesting via bistable systems *Smart Mater. Struct.* **22** 023001

[10] Kuder I K, Arrieta A F and Ermanni P 2015 Design space of embeddable variable stiffness bi-stable elements for morphing applications *Compos. Struct.* **122** 445–455

[11] Shaw A, Neild S, Wagg D, Weaver P and Carrella A 2013 A nonlinear spring mechanism incorporating a bistable composite plate for vibration isolation *J. Sound Vib.* **332** 6265–6275

[12] Ravindran S, Huesgen T, Kroener M and Woias P 2011 A self-sustaining micro thermomechanic-pyroelectric generator *Appl. Phys. Lett.* **99** 104102

[13] Arnaud A, Boughaleb J, Monfray S, Boeuf F, Cugat O and Skotnicki T 2015 Thermo-mechanical efficiency of the bimetallic strip heat engine at the macro-scale and micro-scale *J. Micromechanics Microengineering* **25** 104003

[14] Arya R, Rashid M, Howard D, Collins S and Smith R 2005 Thermally actuated, bistable, oxide/silicon/metal membranes *J. Micromechanics Microengineering* **16** 40

[15] Gowrishetty U R, Walsh K M and Berfield T A 2010 Fabrication of polyimide bi-stable diaphragms using oxide compressive stresses for the field of 'Buckle MEMS' *J. Micromechanics Microengineering* **20** 075013

[16] Kebadze E, Guest S and Pellegrino S 2004 Bistable prestressed shell structures *Int. J. Solids Struct.* **41** 2801–20

[17] Norman A D, Golabchi M R, Seffen K A and Guest S D 2008 Multistable textured shell structures *Adv. Sci. Technol.* **54** 168–173

[18] Norman A D, Seffen K A and Guest S D 2008 Multistable corrugated shells *Proc. R. Soc. A Math. Phys. Eng. Sci.* **464** 1653–72

[19] Loukaides E G and Seffen K A 2015 Multistable grid and honeycomb shells *Int. J. Solids Struct.* **59** 46–57

[20] Ahn S-H, Lee K-T, Kim H-J, Wu R, Kim J-S and Song S-H 2012 Smart soft composite: An integrated 3D soft morphing structure using bend-twist coupling of anisotropic materials *Int. J. Precis. Eng. Manuf.* **13** 631–634

[21] Mirkhalaf M and Barthelat F 2017 Design, 3D printing and testing of architectured materials with bistable interlocks *Extrem. Mech. Lett.* **11** 1–7

[22] Zirbel S A, Tolman K A, Trease B P and Howell L L 2016 Bistable Mechanisms for Space Applications *PLoS One* **11** e0168218

[23] Bauhofer A A, Krödel S, Rys J, Bilal O R, Constantinescu A and Daraio C 2017 Harnessing Photochemical Shrinkage in Direct Laser Writing for Shape Morphing of Polymer Sheets *Adv. Mater.*

[24] Khoo Z X, Teoh J E M, Liu Y, Chua C K, Yang S, An J, Leong K F and Yeong W Y 2015 3D printing of smart materials: A review on recent progresses in 4D printing *Virtual Phys. Prototyp.* **10** 103–122

[25] Mansfield E H 1962 Bending, Buckling and Curling of a Heated Thin Plate *Proc. R. Soc. A Math. Phys. Eng. Sci.* **268** 316–27

[26] Seffen K A 2007 'Morphing' bistable orthotropic elliptical shallow shells *Proc. R. Soc. A Math. Phys. Eng. Sci.* **463** 67–83

[27] Fernandes A, Maurini C and Vidoli S 2010 Multiparameter actuation for shape control of bistable composite plates *Int. J. Solids Struct.* **47** 1449–1458

[28] Seffen K A and Maurini C 2013 Growth and shape control of disks by bending and extension *J. Mech. Phys. Solids* **61** 190–204

[29] Coburn B H, Pirrera A, Weaver P M and Vidoli S 2013 Tristability of an orthotropic doubly curved shell *Compos. Struct.* **96** 446–454

[30] Seffen K A and Guest S D 2011 Prestressed Morphing Bistable and Neutrally Stable Shells *J. Appl. Mech.* **78** 011002

[31] Hamouche W, Maurini C, Vidoli S and Vincenti A 2017 Multi-parameter actuation of a neutrally stable shell: a flexible gear-less motor *Proc. R. Soc. A Math. Phys. Eng. Sci.* **473** 20170364

[32] Loukaides E G, Smoukov S K and Seffen K A 2014 Magnetic actuation and transition shapes of a bistable spherical cap *Int. J. Smart Nano Mater.* **5** 270–82

[33] Vidoli S 2013 Discrete approximations of the Föppl–Von Kármán shell model: From coarse to more refined models *Int. J. Solids Struct.* **50** 1241–1252

[34] Brunetti M, Vincenti A and Vidoli S 2016 A class of morphing shell structures satisfying clamped boundary conditions *Int. J. Solids Struct.* **82** 47–55

[35] Seffen K A and Sobota P Effects of Boundary Conditions on Bistable Behaviour in Axisymmetrical Shallow Shells *Proc. R. Soc. A Math. Phys. Eng. Sci.*

[36] Seffen K A 2008 *Multistable anisotropic shells: governing equations of deformation* (Univ. of Cambridge)

[37] Loukaides E G 2014 *Elementary morphing shells* PhD Thesis (University of Cambridge)

[38] Renishaw 2016 *Material data sheet:Ti6Al4V ELI-0406 powder for additive manufacturing*

[39] Anon *ASM Aerospace Specification Metals Inc., Titanium Ti-6Al-4V (Grade 5), Annealed, Properties*

[40] Khairallah S A, Anderson A T, Rubenchik A and King W E 2016 Laser powder-bed fusion additive manufacturing: Physics of complex melt flow and formation mechanisms of pores, spatter, and denudation zones *Acta Mater.* 36–45

Acknowledgments: We acknowledge a useful discussion on SLS operation with Nneji Kemakolam. We thank Kenneth Nai for assisting in the creation of the spiral structures. Comments by two anonymous reviewers were gratefully received. No external funding contributed to this work.

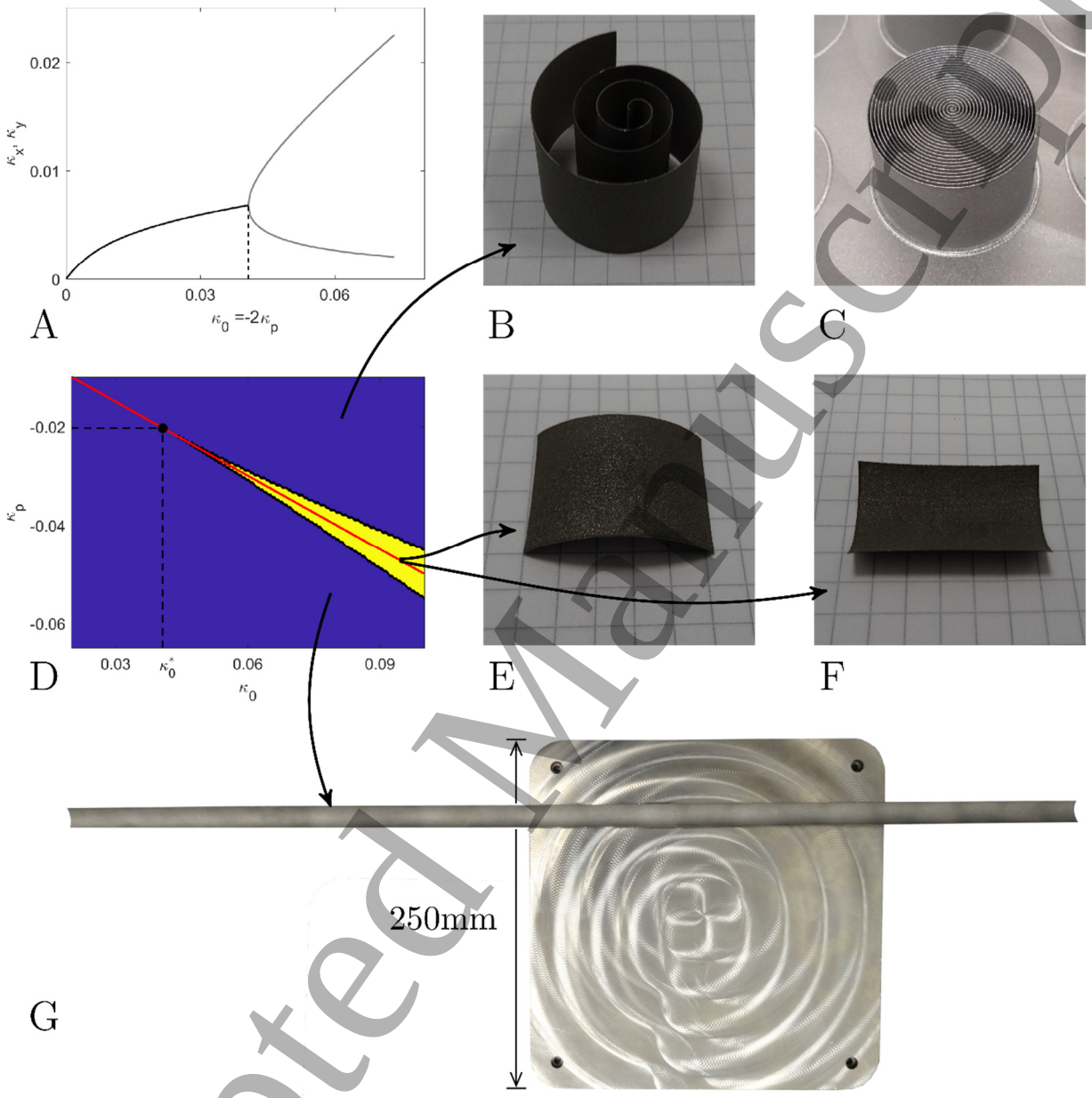

Fig. 1. Analytical solution and emergence of bistability for $\kappa_0 = -2\kappa_p$ (A). Colourmap of monostable (purple) and bistable regions (yellow) for variation of the initial curvature and residual stresses (D). The red line indicates the special case in (A). Titanium spiral after printing and before removal from build plate (C). From this single object, we produced a monostable spiral (B), a bistable shell (E, F) and a monostable part which far exceeds the dimensions of the build plate shown in the same image (G). The lines in the background are spaced at 5mm intervals.

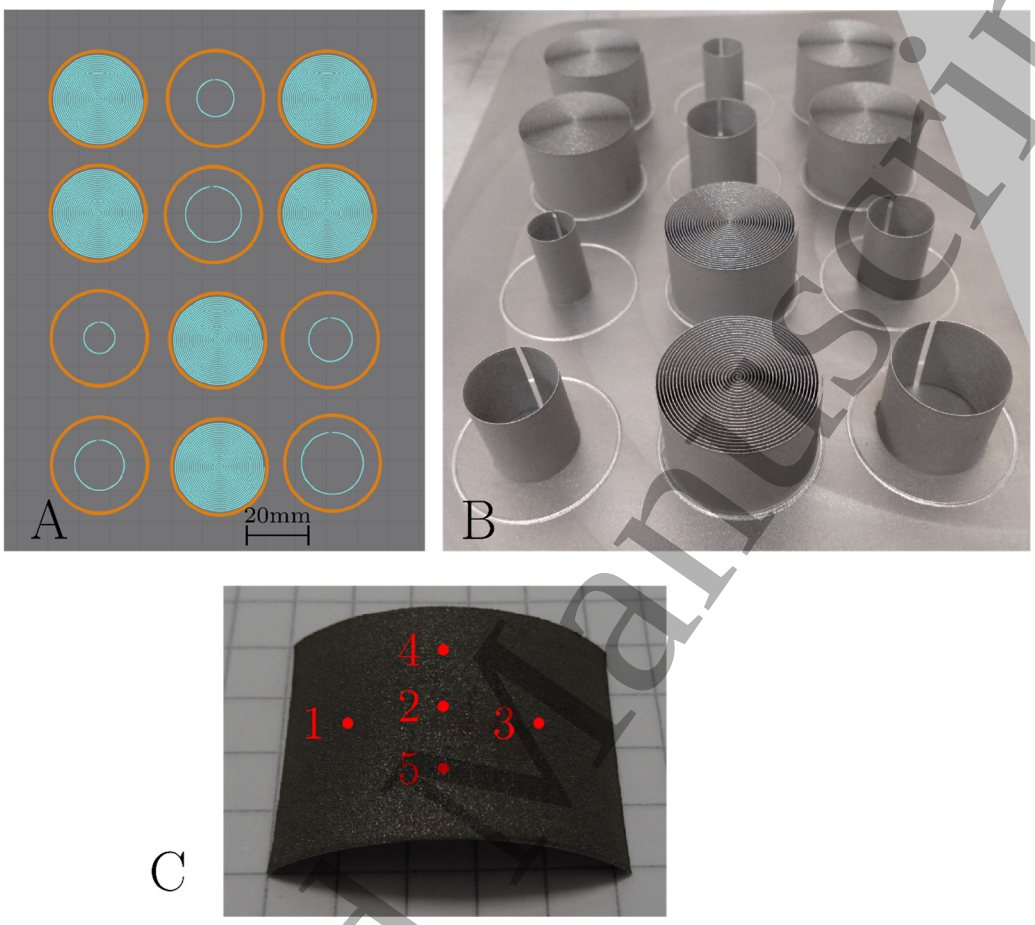

Fig. 2. The geometries and locations of the printed parts as they were designed (A) arranged (B) on the build plate. (C) Locations of XRD measurements on bistable sample.

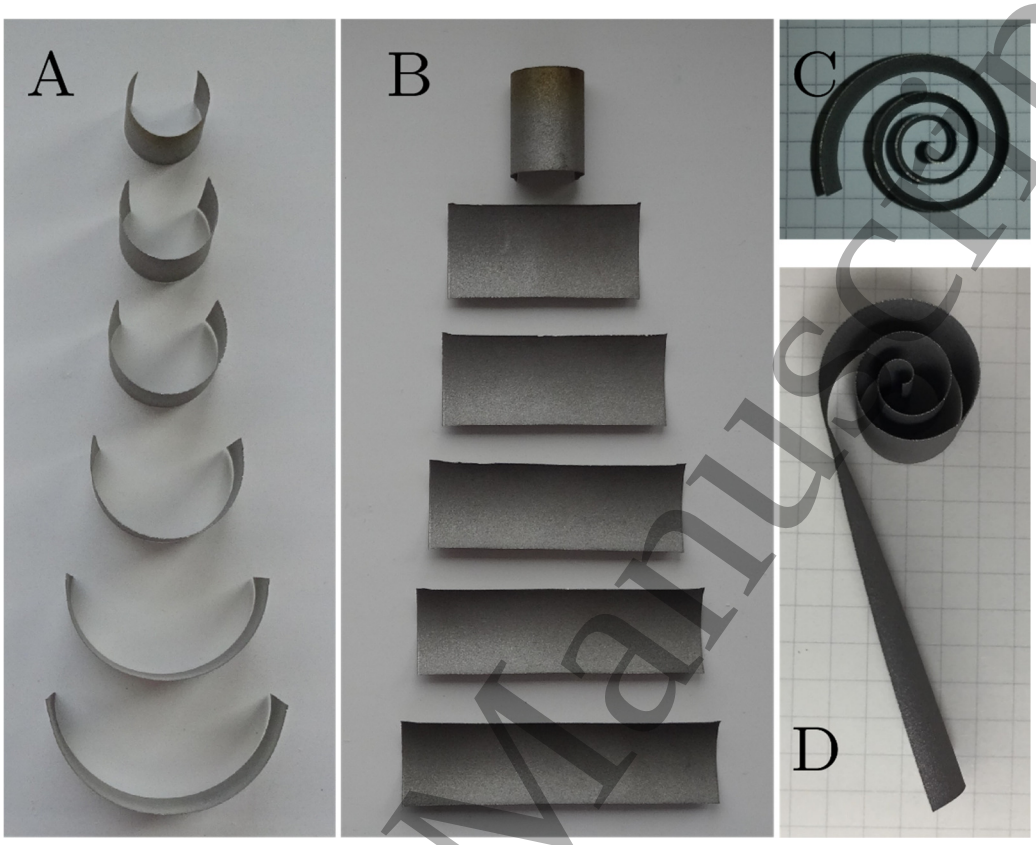

Fig. 3. Printed cylindrical shells of radii 5, 6, 7, 8, 9, 10mm are shown in (A), after removal from the build plate and springback. The same are shown in (B) in secondary stable geometries – except for the monostable highest curvature shell. A 3D-printed spiral shell (C) that demonstrates bistability for the outer section with lower curvature (D), but not for the inner section with higher curvature, thus demonstrating the inherent integration of the two regimes.

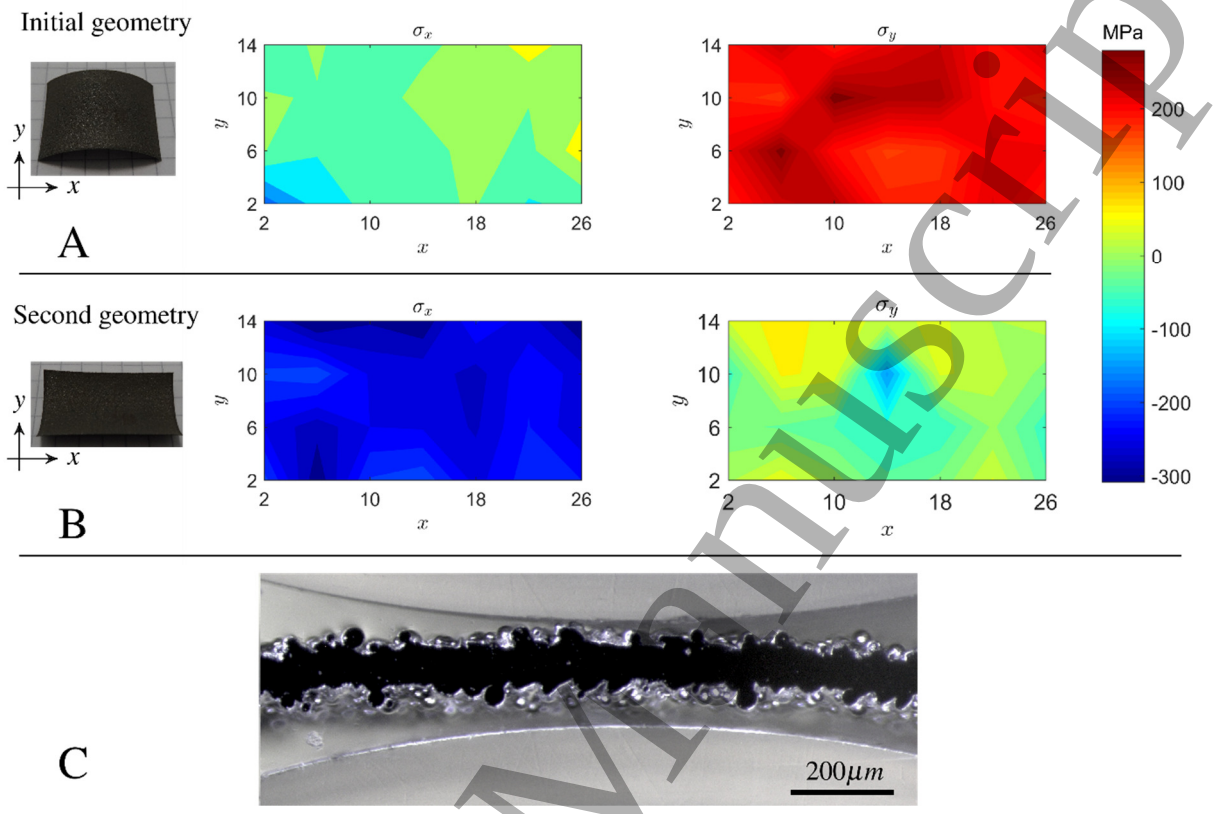

Fig. 4. Residual stresses on the surface of the shell. Measurements using XRD are shown for one side and for (A) the initial geometry and (B) a second stable geometry. (C) shows a cross-section of the sample and the characteristic SLS surface texture.

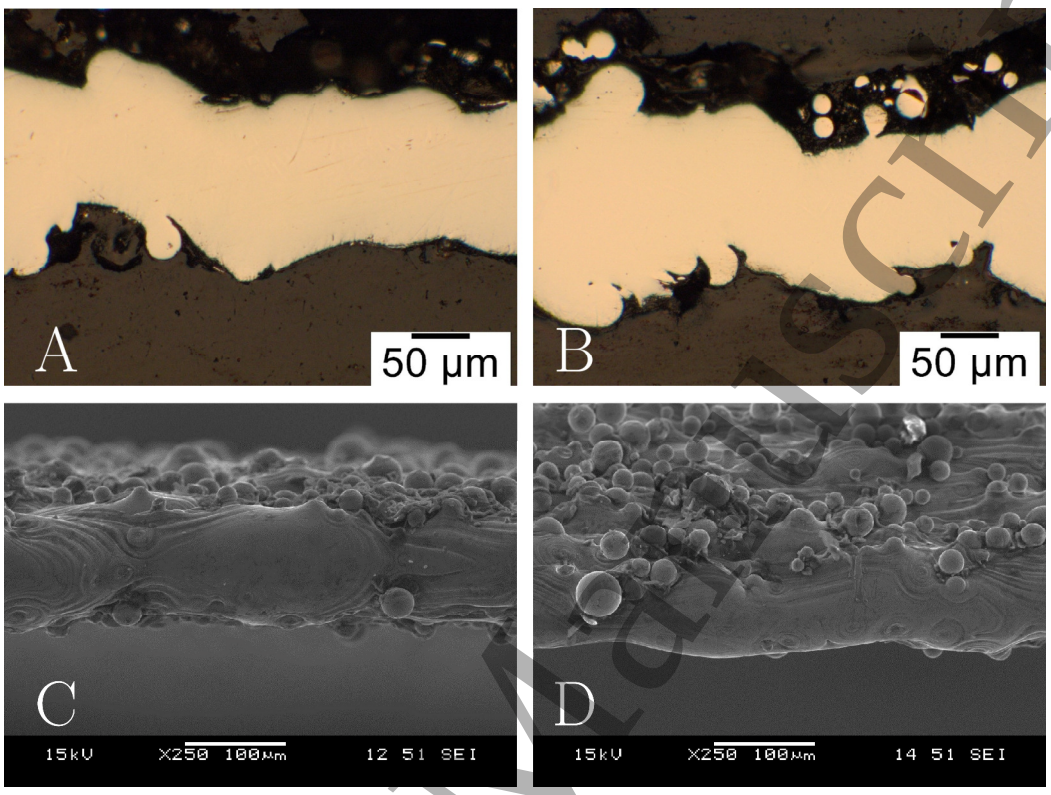

Fig. 5. Microscopy of a through-section of the bistable demonstrator can be seen in (A) and (B). The former section is parallel to the built plate, while the latter is along the height of the component. SEM images show the top surface of the initial geometry (C) and the top surface of the second geometry (D).

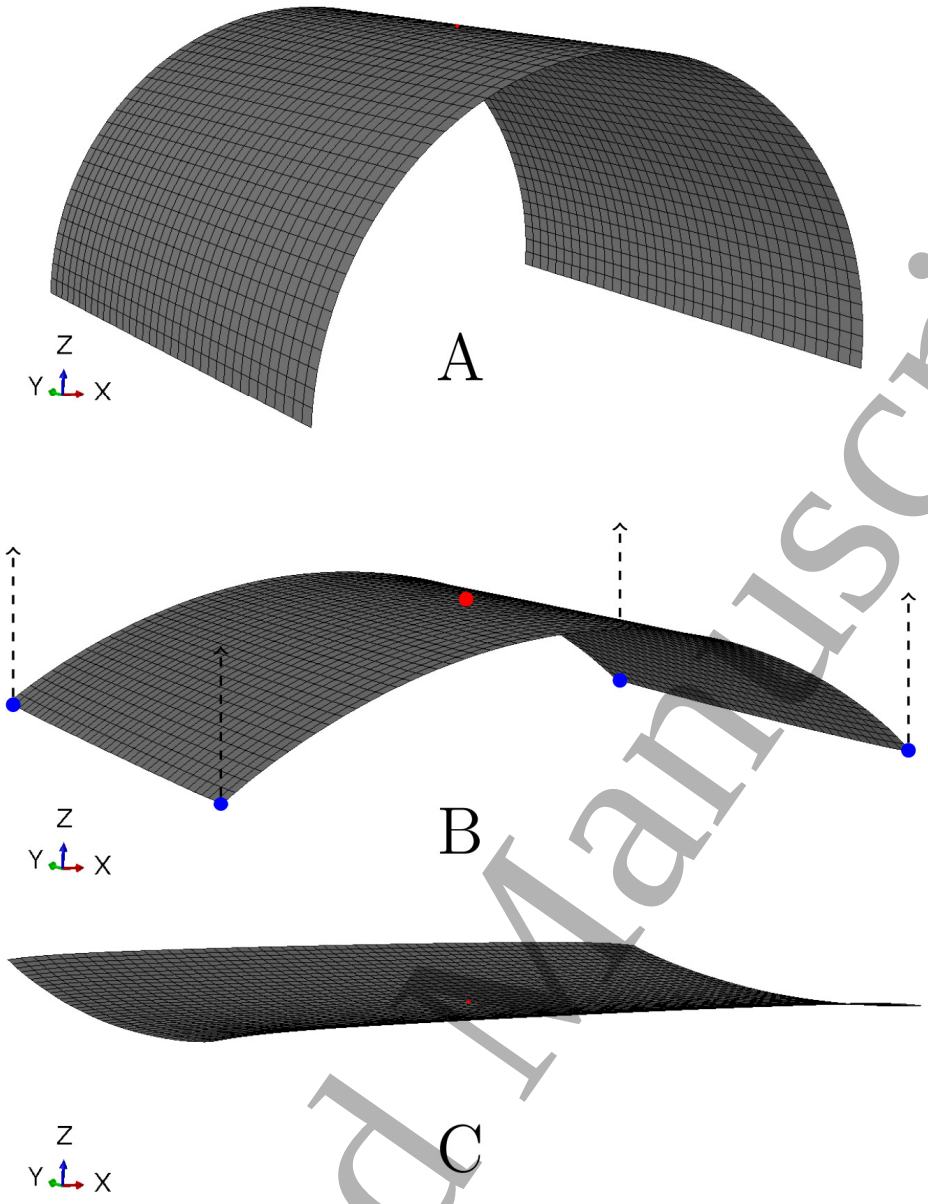

Fig. 6. The FE model in Abaqus. (A) Initial cylindrical geometry; (B) Geometry after thermal stresses are applied, also showing the displacement control on the corner nodes (blue) and the fully constrained centre node (red); (C) Final geometry after boundary conditions are removed and a second stable geometry is revealed.

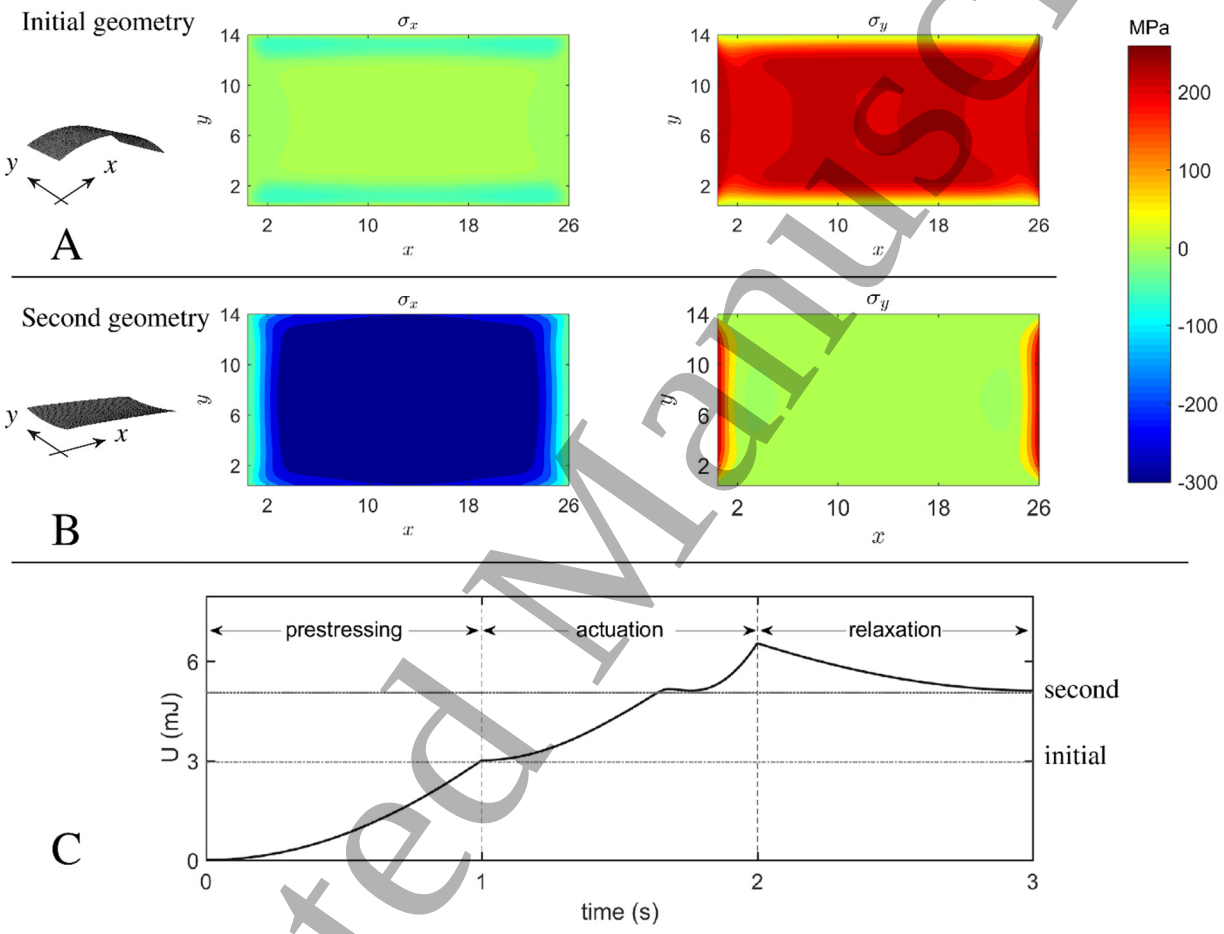

Fig. 7. Finite Element Analysis of a cylindrical shell, showing the stresses on the surface of the shell for top side (as shown on the left) and for (A) a thermally stressed initial geometry and (B) a secondary stable geometry. In (C), the strain energy of the structure is shown for the three steps in the simulation.

Table 1. Residual stresses measured at five locations on the bistable sample using XRD (in MPa). Locations are shown in Fig. 2C and directions refer to Fig. 4. Side 1 is on display in Fig. 4 for both states.

(in MPa)	Initial State				Second State			
	Side 1		Side 2		Side 1		Side 2	
Location	σ_y	σ_x	σ_y	σ_x	σ_x	σ_y	σ_x	σ_y
1	130.3	-28.1	-82.6	-2.7	57	-215.9	77.7	185
2	156.8	-31.8	-46.6	-1.6	33.5	-224.8	77.7	181.8
3	179.2	-23.9	-80.1	4.2	63	-199.8	67.6	185.9
4	144.4	-22.9	-86.8	-6.7	32.5	-212	36	169.1
5	176.4	-37.8	-59.6	-3.5	38.5	-238	90.3	192.4

Table 2. Initial radius of curvature (r_0), final radius of curvature (r_f) after springback and calculated change in curvature for the printed open cylinders.

$\boldsymbol{r_0}$ (mm)	$\boldsymbol{r_f}$ (mm)	$\boldsymbol{\frac{1}{r_0} - \frac{1}{r_f}}$ $(\mathbf{10^{-2} mm^{-1}})$
5	6.51	4.65
6	8.55	4.98
7	10.16	4.45
8	11.47	3.78
9	16.16	4.92
10	19.02	4.74